pH-Responsive Cyanine-Grafted Graphene Oxide for Fluorescence Resonance Energy Transfer-Enhanced Photothermal Therapy

Miao Guo, Jie Huang, Yibin Deng, He Shen, Yufei Ma, Mengxin Zhang, Aijun Zhu, Yanli Li, He Hui, Yangyun Wang, Xiangliang Yang, Zhijun Zhang, and Huabing Chen**

Stimuli-responsive anticancer agents are of particular interest in the field of cancer therapy. Nevertheless, so far stimuli-responsive photothermal agents have been explored with limited success for cancer photothermal therapy (PTT). In this work, as a proof-of-concept, a pH-responsive photothermal nanoconjugate for enhanced PTT efficacy, in which graphene oxide (GO) with broad NIR absorbance and effective photothermal conversion efficiency is selected as a typical model receptor of fluorescence resonance energy transfer (FRET), and grafted cyanine dye (e.g., Cypate) acts as the donor of near-infrared fluorescence (NIRF), is reported for the first time. The conjugate of Cypate-grafted GO exhibits different conformations in aqueous solutions at various pH, which can trigger pH-dependent FRET effect between GO and Cypate and thus induce pH-responsive photothermal effect of GO-Cypate. GO-Cypate exhibits severe cell damage owing to the enhanced photothermal effect in lysosomes, and thus generate synergistic PTT efficacy with tumor ablation upon photoirradiation after a single-dose intravenous injection. The photothermal nanoconjugate with broad NIR absorbance as the effective receptor of FRET can smartly convert emitted NIRF energy from donor cyanine dye into additional photothermal effect for improving PTT. These results suggest that the smart nanoconjugate can act as a promising stimuli-responsive photothermal nanoplatform for cancer therapy.

1. Introduction

Photothermal therapy (PTT) is a non-invasive modality for treating cancer, which utilizes photo-absorbing agents including carbon nanomaterials (e.g., graphene oxide, GO), gold nanoparticles, and organic near-infrared (NIR) dyes (e.g., cyanine) to generate a high localized temperature for ablating tumor without damaging surrounding healthy tissues under NIR light irradiation.[1] These photothermal agents exhibit good photothermal conversion efficiency to generate significant hyperthermia upon NIR irradiation.[1a,d] Recently, it is highly desired to explore new strategies to improve photothermal effect of these agents for enhanced PTT efficacy. For instance, several gold nanostructures with different dimensions are designed to optimize their photothermal conversion efficiency,[2] and reduced graphene oxide-coated gold nanorods are found to possess an enhanced photothermal effect for superior PTT.[3] Additionally, the nanocarriers are also employed to improve the accumulations of photothermal agents such as cyanine dyes at tumors via enhanced permeation and retention (EPR) effect, which can improve their photothermal efficacy owing to the concentration-dependent hyperthermia.[4] Despite recent exciting progress in the development of various photothermal agents,[5] there are only a few strategies to improve the intrinsic photothermal performance of photothermal agents owing to the absence of strategies to regulate their photothermal conversion efficiency in addition to dimensions

M. Guo, Dr. Y. B. Deng, A. J. Zhu, Y. L. Li, Dr. H. Hui, Prof. H. B. Chen
Jiangsu Key Laboratory of Translational Research and Therapy for Neuro-Psycho-Diseases and College of Pharmaceutical Sciences
Soochow University
Suzhou 215123, Jiangsu, China
E-mail: chenhb@suda.edu.cn

J. Huang, H. Shen, Y. F. Ma, M. X. Zhang, Prof. Z. J. Zhang
Key Laboratory of Nano-Bio Interface
Division of Nanobiomedicine
Suzhou Institute of Nano-Tech and Nano-Bionics
Chinese Academy of Sciences
Suzhou 215123, Jiangsu, China
E-mail: zjzhang2007@sinano.ac.cn

DOI: 10.1002/adfm.201402762

Dr. Y. Y. Wang, Prof. H. B. Chen
School for Radiological & Interdisciplinary Sciences (RAD-X)
Collaborative Innovation Center of Radiation Medicine of Jiangsu Higher Education Institutions, and School of Radiation Medicine and Protection
Soochow University
Suzhou 215123, Jiangsu, China

Prof. X. L. Yang
National Engineering Research Center for Nanomedicine, and College of Life Science and Technology
Huazhong University of Science and Technology
Hubei, Wuhan 430074, China

© 2014 WILEY-VCH Verlag GmbH & Co. KGaA, Weinheim

and concentrations.[3] Moreover, so far there is still no report about smart photothermal agents for improving PTT,[6,7] although stimuli-responsive chemistry has extensively been used to achieve smart drug release in the field of drug delivery. It is highly necessary to develop smart photothermal agents to improve their intrinsic photothermal performances for enhanced PTT.

Despite the existing inorganic photothermal agents,[7,8] organic NIR cyanine dyes such as indocyanine green and Cypate have been explored as clinically potential photothermal agents without safety concern in our previous work,[4,9] which can convert absorbed optical energy into thermal effect via the non-radiative transition upon NIR light irradiation.[1d,9,10] However, this type of cyanine dyes can often generate near-infrared fluorescence (NIRF) via their radiative transition in photothermal conversion process upon photoirradiation as well. Obviously, their photothermal conversion efficiency is remarkably dissipated owing to the generation of radiative transition-mediated NIRF. Most interestingly, photothermal inorganic nanoparticles with broad absorbance such as GO can act as receptor to receive fluorescence from fluorescent dyes as donor in the presence of fluorescence resonance energy transfer (FRET).[11] Presumably, NIRF from cyanine dyes might be converted into additional thermal energy using photothermal inorganic agents with broad NIR absorbance in addition to their original photothermal performances upon the formation of FRET between cyanine dyes and photothermal inorganic agents. Thus, the regulation of FRET may play a key role in the generation of additional photothermal energy source for enhanced PTT. Herein, as a proof-of-concept, we report a pH-responsive Cypate-grafted GO nanoconjugate (GO-Cypate) system exhibiting FRET effect between Cypate and GO (**Scheme 1**), in which GO with broad NIR absorbance is selected as a typical model receptor owing to its effective photothermal conversion efficiency, high drug loading capacity, and targeting ability. Particularly, GO-Cypate exhibits the enhanced photothermal effect in acidic environment owing to pH-dependent FRET effect between GO and Cypate. GO-Cypate can be internalized into the lysosomes via clathrin-mediated endocytosis and thus induce enhanced photothermal cell damage via pH-responsive photothermal effect. Moreover, GO-Cypate possesses the good accumulation at tumor and finally results in synergistic PTT efficacy with tumor ablation upon NIR irradiation after a single-dose intravenous injection.

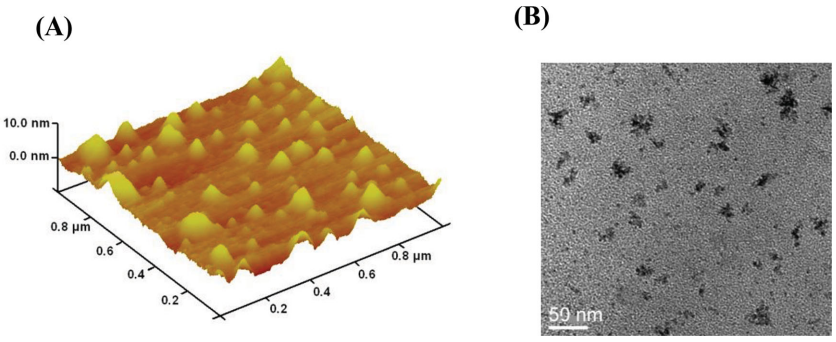

Figure 1. A) AFM image of GO-Cypate (average thickness, 3.2 ± 0.9 nm). B) TEM image of GO-Cypate (average size, 24.5 ± 6.5 nm).

2. Results and Discussion

2.1. Synthesis and Characterization

2.1.1. Synthesis of GO-Cypate

In order to synthesize GO-Cypate, GO was prepared according to literature.[8] Then, six-armed amine-terminated polyethylene glycol (PEG) was reacted with GO to give PEG-modified GO (GO-PEG) via carbodiimide-catalyzed amide formation and further covalently coupled with Cypate, followed by ultrafiltration through a 100-kDa filter (Millipore) for the purification of GO-Cypate with the loading of 23% Cypate.[9,12] Atomic force microscopy (AFM) images indicate that GO-PEG and GO-Cypate had the average thickness of 1.5 ± 0.7 nm and 3.2 ± 0.9 nm, respectively, indicating that GO-Cypate consisted of the mixture of single- and double-layered sheets (**Figure 1** and Supporting Information Figure S1). Transmission electron microscopy (TEM) imaging indicates that GO-Cypate had the average size of 24.5 ± 6.5 nm (Figure 1). GO-Cypate exhibited the absorbance peak at 783 nm, and fluorescence peak at 815 nm in the emission range of 810–850 nm in methanol solution, confirming the successful conjugation of GO-Cypate (**Figure 2**A and 2B).

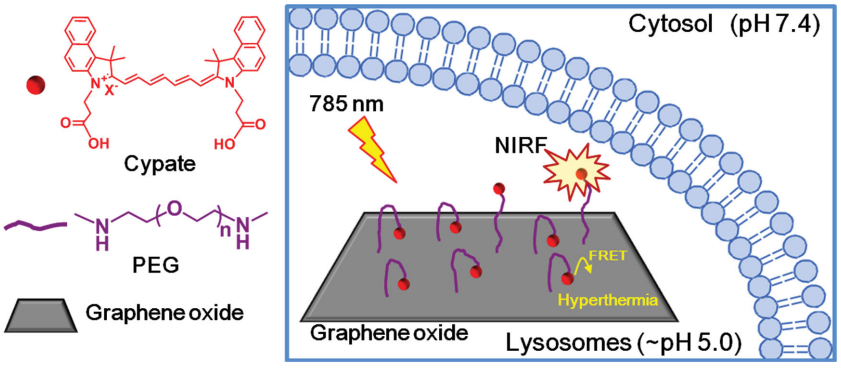

Scheme 1. Schematic illustration of smart GO-Cypate nanoconjugate exhibiting enhanced photothermal performance mediated by pH-dependent FRET.

2.1.2. Conformations of GO-Cypate in Solvents

We further found that GO-Cypate had stronger fluorescence in methanol than that in de-ionized water, indicating that GO-Cypate was obviously quenched in aqueous solution, but recovered in methanol, a good solvent for Cypate (Figure 2B). Presumably, Cypate as a hydrophobic dye was quenched owing to fluorescence resonance energy transfer (FRET) from Cypate to GO, a highly efficient fluorescence quencher.[11b] In order

© 2014 WILEY-VCH Verlag GmbH & Co. KGaA, Weinheim

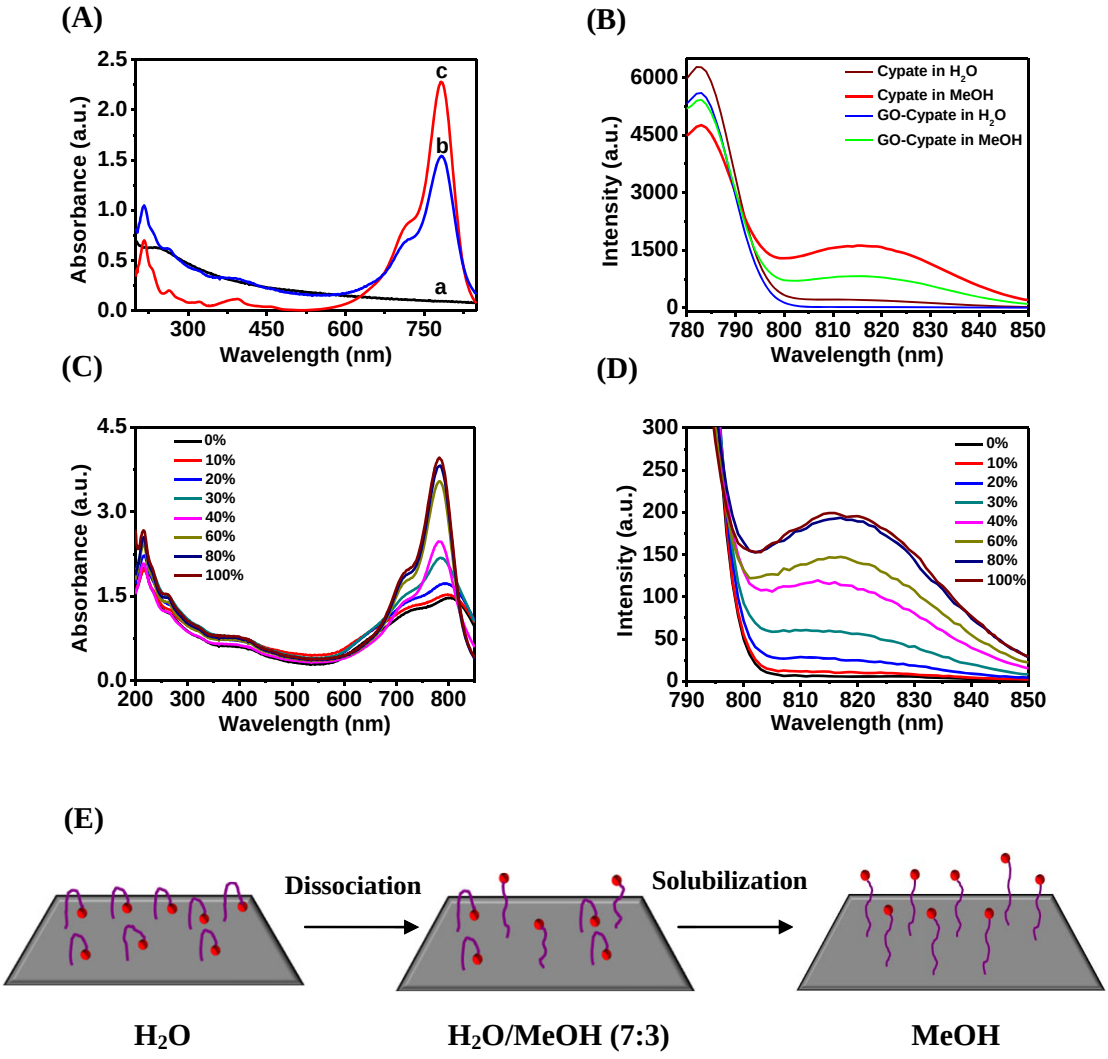

Figure 2. A) UV–Vis spectra of a) GO-PEG in aqueous solution, b) GO-Cypate in aqueous solution, and c) Cypate in methanol. B) Fluorescence spectra of GO-Cypate and Cypate in aqueous solution and methanol, respectively. C) UV–Vis spectra and D) Fluorescence spectra of GO-Cypate (10.0 μg mL^{-1}) in aqueous solution containing various percentages of methanol. E) Conformation illustration of GO-Cypate in various solvents (Cypate exists as aggregates on GO surface in H_2O, Cypate aggregates dissociate on GO surface in H_2O/MeOH (7:3), and finally Cypate molecules depart from GO surface upon more solubilization in MeOH).

to understand the quenching mechanism of Cypate on GO, UV–Vis and fluorescent spectra of GO-Cypate (10.0 μg mL^{-1} Cypate) were measured in mixed methanol-water solutions (Figure 2C,D). When the percentages of methanol were increased from 0% to 30%, GO-Cypate exhibited gradual increase of absorbance and fluorescence intensities, and blue shift of the characteristic absorbance peak from 801 nm to 783 nm (Figure 2C,D), which possibly resulted from the dissociation of Cypate aggregates on the surface of GO.[12b] However, GO-Cypate showed no shift of the characteristic absorbance peak, and only displayed the increases of absorbance and fluorescence in the presence of 40% methanol or higher percentages (Figure 2C,D), implying that these increases might not result from the dissociation of Cypate aggregates on the surface of GO. We presumed that the increase in the absorbance of GO-Cypate without peak shift attributes to the gradual solubilization and thereof loose of Cypate on the surface of GO in methanol solution, which can trigger the diminishing of FRET.[13] Then, we propose that Cypate molecules might exist as the aggregates on the surface of GO in aqueous solution, which may be dissociated and further departed from the surface of GO upon solubilization (Figure 2E).[13] The lifetime of GO-Cypate in various solutions was further evaluated to demonstrate the conformation of Cypate on the surface of GO as shown in Figure 2E. The lifetime of GO-Cypate was prolonged from 0.11 ns to 0.37 ns upon solubilization by methanol (Table S1, Supporting Information), indicating the presences of Cypate aggregates and FRET between Cypate and GO. To probe the conformation of Cypate on the surface of GO in aqueous solutions, we further evaluated the fluorescent spectra and lifetime of GO-Cypate in aqueous solutions at various pH. GO-Cypate exhibited enhanced fluorescence intensities in PBS

© 2014 WILEY-VCH Verlag GmbH & Co. KGaA, Weinheim

when pH was changed from 5.0 to 8.0 (Figure S2, Supporting Information). The lifetime of GO-Cypate was also prolonged from 0.15 ns to 0.40 ns when pH was increased from 5.0 to 8.0 (Table S1, Supporting Information). The enhanced fluorescence intensity and lifetime of GO-Cypate may result from the partial de-protonation in physiological pH (e.g., pH 7.4), which triggers the departure of Cypate from the surface of GO in PBS and thereof diminishing of FRET between Cypate and GO. The lifetime data also indicate that GO-Cypate at pH 5.0 and 8.0 has the similar conformations to those in 30% and 100% methanol solutions, respectively, as shown in Figure 2E, and the conformation of GO-Cypate at pH 5.0 is highly advantageous to the generation of FRET than those above pH 5.0.

2.1.3. Stability of GO-Cypate

GO was found to be able to improve the chemical stability and photostability of hydrophobic compounds adsorbed to GO in the existing studies.[14] Given that photostability greatly affects UV absorbance of organic dye, we evaluated the capability of GO to improve the photostability of Cypate. UV–Vis spectra show that free Cypate exhibited quick disappearance of absorbance under 785 nm photoirradiation within 5 min, presumably owing to its rapid photobleaching (**Figure 3**A). GO-Cypate still exhibited sufficient absorbance (Figure 3B), even though GO-Cypate also had a remarkable loss of absorbance under 785 nm photoirradiation during 10 min. It indicates that GO can significantly improve the photostability of cyanine dye (Figure 3C), which is advantageous to the generation of the fluorescence or photothermal effect from Cypate.[14a] Moreover, we evaluated the stability of the conjugated Cypate on the surface of GO in culture medium containing 10% fetal bovine serum (FBS) by observing the release of Cypate from GO-Cypate, and found that only a negligible amount of free Cypate was released in medium, and GO-Cypate exhibited no remarkable cleavage of the covalent bond between Cypate and GO in the medium (Figure S3, Supporting Information). Additionally, we also evaluated the colloidal stability of GO-Cypate in various solutions using centrifuge test (12 000 rpm, 10 min). It indicates that GO-Cypate exhibited good physical stability in H_2O, PBS, and culture medium containing FBS.

2.1.4. FRET-Mediated Photothermal Effect of GO-Cypate

To demonstrate the photothermal effect of GO-Cypate, we firstly evaluated the photothermal capacities of GO-Cypate with the loading levels of 2.9%, 6.5%, and 23% Cypate on the surface of GO in aqueous solutions (Figure 3D). GO-Cypate containing 23% Cypate (16.5 μg mL^{-1} GO and 5.0 μg mL^{-1}) exhibited a quick temperature increase of 33 °C during 300 s under 1.5 W cm^{-2} 785 nm photoirradiation, which is much superior to GO-PEG and GO-Cypate with 2.9% and 6.5% Cypate (Figure 3D). Moreover, even at lower concentrations (3.3 μg mL^{-1} GO and 1.0 μg mL^{-1} Cypate), GO-Cypate still displayed a significant increase of 8 °C in temperature during 120 s (Figure S4, Supporting Information). Obviously, GO-Cypate with the chemistry design of donor-receptor system can provide the additional energy source from the fluorescence energy of Cypate via FRET effect in addition to the thermal energy from GO. It also indicates that the enhanced photothermal effect of GO-Cypate is highly dependent on the number of conjugated Cypate on the surface of GO.[3a] In addition, the broad absorbance of GO can facilitate GO to absorb most of NIRF in the wavelength range of 810–850 nm, and thus maximize the conversion efficiency of NIRF into thermal energy.

In order to validate the conformations of GO-Cypate with FRET in aqueous solutions as shown in Figure 2E, we further evaluated the photothermal effects of GO-PEG and GO-Cypate with 23% Cypate at various pH (Figure 3E,F). It indicates that GO-Cypate at pH 5.0 exhibited much higher increase of temperature than those at pH 7.4 and 8.0 under photoirradiation. GO-Cypate at pH 5.0 had a temperature increase of ~8 °C as compared to that at pH 7.4 during 300 s. However, GO-PEG as the control had the negligible change of temperature at various pH. Obviously, GO-Cypate displayed the pH-responsive photothermal effect, which is highly correlated to its lifetime and thereof FRET status at various pH (Table S1, Supporting Information). Therefore, GO-Cypate exhibits an enhanced FRET effect between GO and Cypate at acidic environment as shown in Figure 3G. These results indicate that GO-Cypate is able to quickly trigger the photothermal effect during a short photoirradiation, and also intensify hyperthermia (above 42 °C) at acidic environment (e.g., lysosomal pH) as compared to that at pH 7.4. The enhanced photothermal effect of GO-Cypate in lysosomal environment may play a key role for inducing more severe cell injury if GO-Cypate can be internalized into lysosomes.

2.2. In Vitro Cell Studies of GO-Cypate

2.2.1. Cell Uptakes and Intracellular Distribution

To demonstrate whether GO-Cypate can be internalized by cancer cells, we evaluated their cellular uptake by murine 4T1 breast cancer cells. GO-Cypate results in 3-fold and 4-fold increases of the cellular uptake of Cypate after 6 h and 24 h incubation, respectively (**Figure 4**A), indicating that GO-Cypate easily interacted with the cells. It is likely that the enhanced internalization is caused by the positive charge of GO-Cypate (10.5 mV). Subsequently, the endocytic pathways of rhodamine B isothiocyanate (RBITC)-labeled GO-Cypate were further investigated using several inhibitors of endocytosis including chlorpromazine (CPZ), methyl-β-cyclodextrin (MβCD), amiloride and sodium azide. Figure S5 shows that CPZ as an inhibitor of clathrin-mediated endocytosis resulted in the decrease of 41% fluorescence intensity, suggesting that GO-Cypate was mainly internalized via a clathrin-mediated endocytic pathway. Clathrin-mediated endocytosis was reported to play a major role in internalization of the nanoparticles into cancer cells.[15] In addition, sodium azide also led to a significant decrease of cellular uptake, indicating that the endocytic cellular uptake is an energy-dependent process.[16] The clathrin-mediated pathway allows GO-Cypate to undergo endolysosomal transport for their intracellular delivery.[15] These results also accord with our previous study on the endocytosis mechanism of GO.[17] Moreover, we further employed confocal laser scanning microscopy (CLSM) to observe the intracellular distribution of RBITC-labeled GO-Cypate in 4T1 cells. The

© 2014 WILEY-VCH Verlag GmbH & Co. KGaA, Weinheim

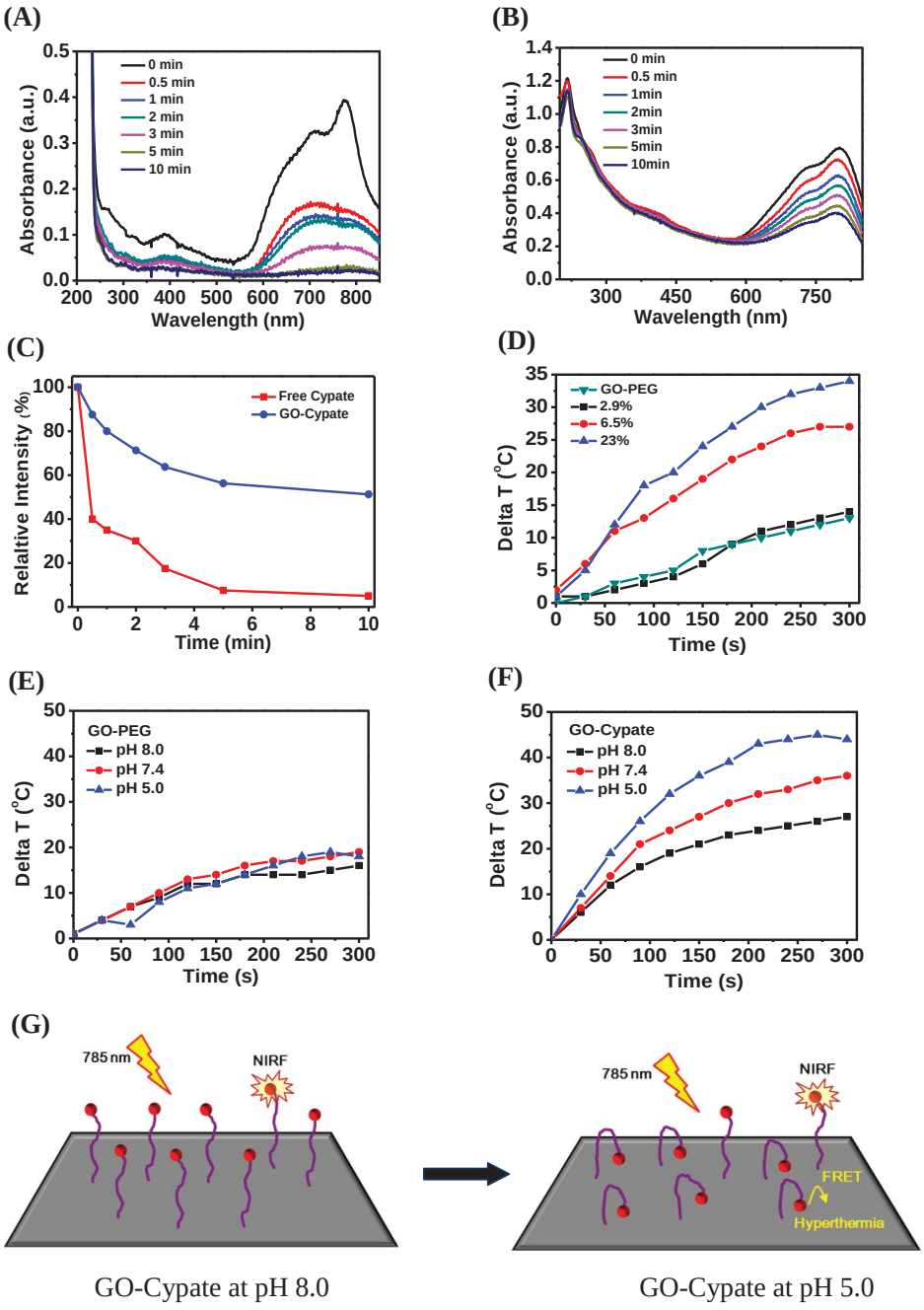

Figure 3. A) UV–Vis spectra of free Cypate in aqueous solutions (5.0 μg mL^{-1}) exposed to 1.5 W cm^{-2} 785 nm photoirradiation at different time, respectively. B) UV–Vis spectra of GO-Cypate (16.5 μg mL^{-1} GO, and 5.0 μg mL^{-1} Cypate) in aqueous solution under 1.5 W cm^{-2} photoirradiation at different time, respectively. C) Normalized UV–Vis absorbances of GO-Cypate and free Cypate at 783 nm at different time according to the data from (A,B). D) Photothermal effects of GO-PEG (16.5 μg mL^{-1} GO), and GO-Cypate with various loading levels of Cypate (16.5 μg mL^{-1} GO/2.9%, 6.5%, and 23% Cypate, respectively) in purified water (0.5 mL) within 5 min photoirradiation. E) Photothermal effects of GO-PEG (16.5 μg mL^{-1} GO) in the buffers at pH 5.0, 7.4 and 8.0 within 5 min photoirradiation, respectively. F) Photothermal effects of GO-Cypate (16.5 μg mL^{-1} GO, and 5.0 μg mL^{-1} Cypate) in the buffers at pH 5.0, 7.4 and 8.0 within 5 min photoirradiation, respectively. G) Conformation illustration of GO-Cypate at various pH and thereof FRET between GO and Cypate.

lysosomes were stained by CellLight Lysosomes-GFP, a modified insect virus expressing a fusion construct of TagGFP and lysosomal associated membrane protein 1 (Lamp 1 protein) after the incubation of 4T1 cells with RBITC-labeled GO-Cypate for 4 h. Figure 4B shows that GO-Cypate had a good co-localization in the lysosomes, indicating GO-Cypate is preferably internalized into the lysosomes via clathrin-mediated endocytosis,[9] in which GO-Cypate is able to exhibit enhanced photothermal effect in the lysosomes owing to the enhanced FRET at pH 5.0. Thus, the distribution of GO-Cypate into the lysosomes is potentially advantageous to trigger the enhanced photothermal cell damage owing to the enhanced photothermal effect.

© 2014 WILEY-VCH Verlag GmbH & Co. KGaA, Weinheim

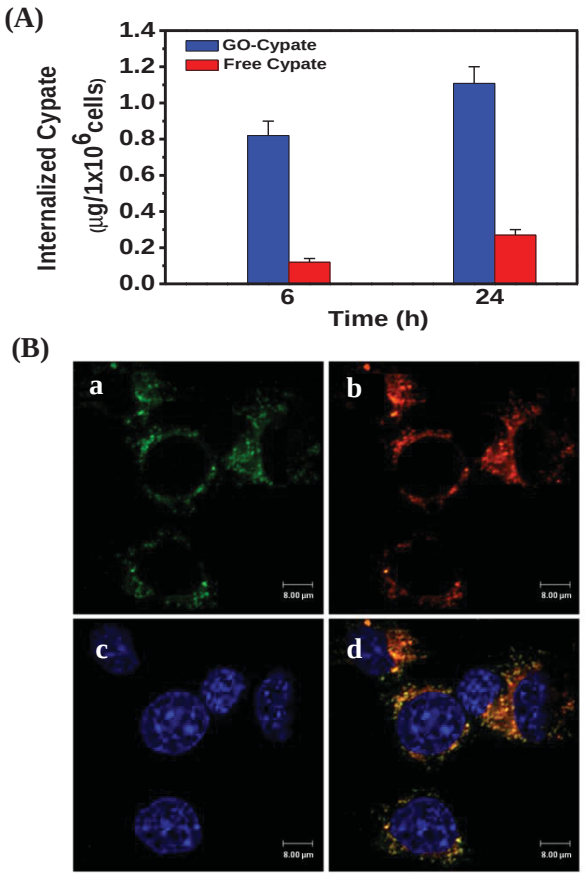

Figure 4. A) Amounts of internalized Cypate from free Cypate and GO-Cypate by 4T1 cells after 6 h and 24 h incubation at the dose of 10.0 μg mL^{-1} Cypate, respectively. B) Confocal fluorescent images of 4T1 cells stained by CellLight Lysosomes-GFP after 4 h incubation with RBITC-labeled GO-Cypate. a) Lysosomes stained by CellLight Lysosomes-GFP, b) RBITC-labeled GO-Cypate with red fluorescence, c) Nucleus stained by Hoechst 33342, d) Co-localization of RBITC-labeled GO-Cypate within the lysosomes.

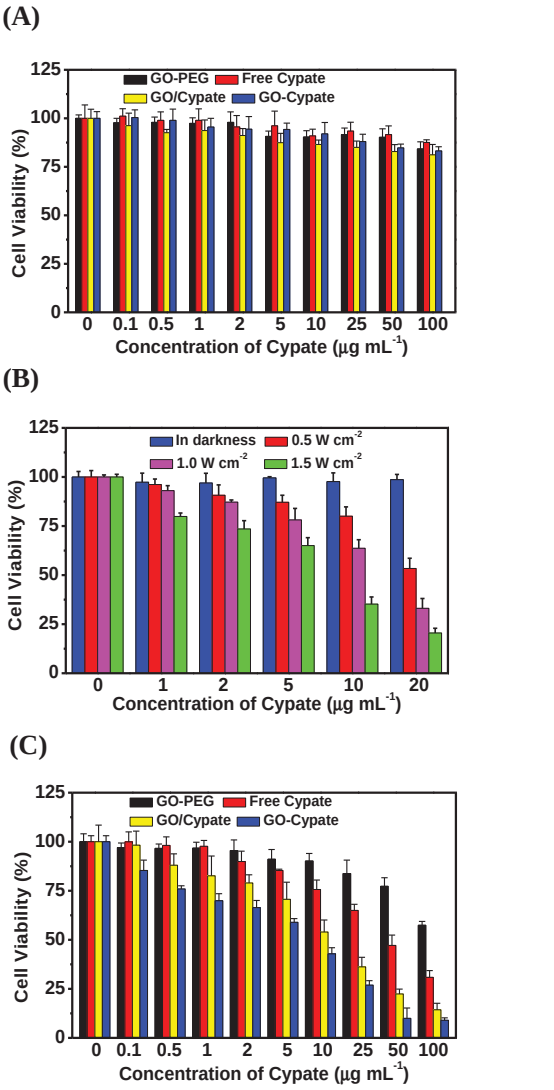

Figure 5. A) Cell viability of 4T1 cells treated with GO-Cypate, GO-PEG and free Cypate at various concentrations of Cypate in the darkness. B) Cell viability of 4T1 cells treated with GO-Cypate at various concentrations under darkness, 0.5 W cm^{-2}, 1.0 W cm^{-2}, and 1.5 W cm^{-2} photoirradiation (3 min), respectively. C) Cell viability of 4T1 cells treated with GO-Cypate, GO-PEG and free Cypate at various concentrations of Cypate under 1.5 W cm^{-2} 785 nm PTT treatments for 3 min.

2.2.2. Photocytotoxicity

To examine the photothermal injury of GO-Cypate on cancer cells, we incubated 4T1 cells with various formulations for 24 h, followed by 3 min photoirradiation at various intensities. GO-Cypate, GO-PEG and free Cypate exhibited no significant cytotoxicity in the absence of photoirradiation (**Figure 5**A). However, GO-Cypate exhibited an irradiation intensity-dependent cytotoxicity against 4T1 cells (Figure 5B), and had much stronger cytotoxicity with the IC_{50} value of 6.0 μg mL^{-1} upon PTT treatment (3 min, 1.5 W cm^{-2}). It indicates that GO-Cypate exhibited much higher cytotoxicity than GO-PEG and free Cypate under PTT treatment (Figure 5C). In contrast, the physical mixture of free Cypate and GO-PEG (GO/Cypate) exhibited a higher IC_{50} value (about 11.0 μg mL^{-1}) under the same PTT treatment. It indicates that GO-Cypate via the conjugation can potentially trigger much more severe photothermal injury to cancer cells via the enhanced cellular uptake and photothermal performance. In particular, GO/Cypate as the physical mixture of GO-PEG and Cypate exhibited a less cytotoxicity than GO-Cypate with the conjugation chemistry, implying that the enhanced cytotoxicity of GO-Cypate might attribute to the additional photothermal effect from the energy transfer of NIRF from Cypate.

2.3. In Vivo Studies of GO-Cypate

2.3.1. Biodistribution

To demonstrate the in vivo biodistribution behavior of GO-Cypate, we injected GO-Cypate intravenously into the mice bearing murine 4T1 tumor and evaluated the accumulative amounts of Cypate from GO-Cypate in various tissues (**Figure 6**A) using UV–Vis analysis, and ex vivo NIRF intensities

© 2014 WILEY-VCH Verlag GmbH & Co. KGaA, Weinheim

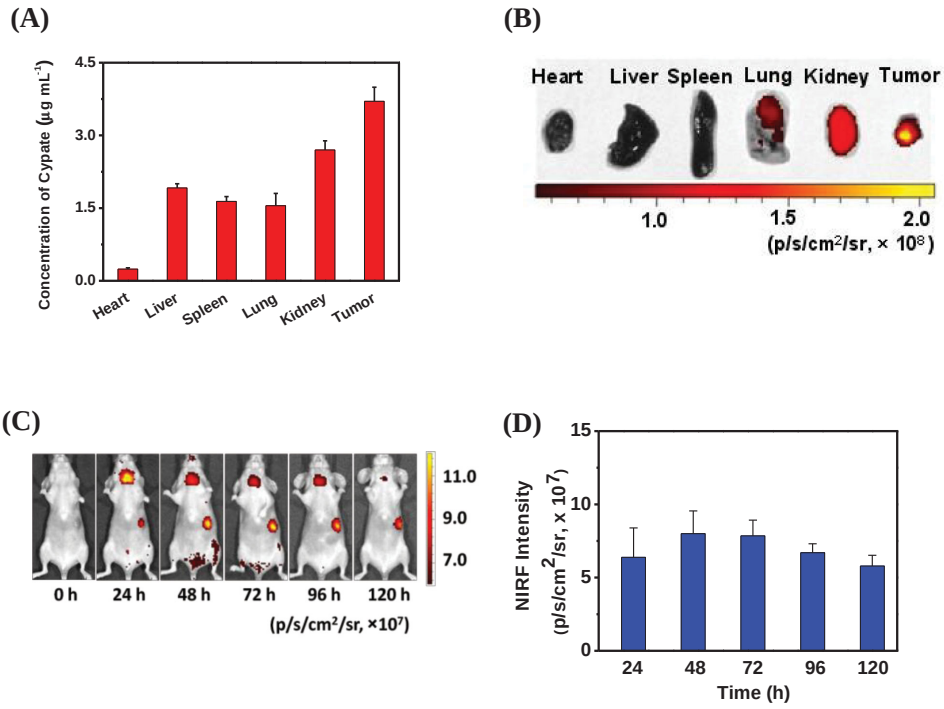

Figure 6. A) Accumulative amounts and B) ex vivo image of Cypate from GO-Cypate in heart, liver, spleen, lung, kidney, and tumor of the mice bearing 4T1 tumor at 24 h post-injection at the dose of 7.5 mg kg^{-1} GO-Cypate. C) In vivo NIRF images and D) its NIRF intensities of the mice bearing 4T1 tumor injected with GO-Cypate at the dose of 7.5 mg kg^{-1} GO-Cypate at 0, 24, 48, 72, 96 and 120 h post-injection, respectively.

of GO-Cypate in various tissues at 24 h post-injection (Figure 6B and Supporting Information Figure S6). Figure 6A,B show that GO-Cypate accumulated in the tumor, liver, and kidney at 24 h post-injection, and particularly exhibited good accumulation in the tumor possibly owing to the enhanced permeability and retention (EPR) effect.[9,18] The preferable targeting capacity of GO-Cypate to tumor site provides a key prerequisite for superior PTT efficacy.

To further demonstrate the targeting capacity of GO-Cypate, we further evaluated the in vitro NIRF imaging of 4T1 cells. GO-Cypate exhibited a relatively prolonged retention of NIRF signals in 4T1 cells without significant cytotoxicity during the imaging period of 3 days (Figure S7, Supporting Information). It implies that GO-Cypate is able to be internalized and retained within the cells without obvious exocytosis during a relatively long-term imaging period. Subsequently, we evaluated the in vivo NIRF imaging of GO-Cypate on the mice bearing 4T1 tumors. GO-Cypate exhibited the tumor accumulation of NIRF signals from Cypate at 24 h post-injection (Figure 6C,D), which is consistent with the data from Figure 6A. In particular, the NIRF signals were slightly increased and reached a plateau at 48 h post-injection.[11b,13] Moreover, GO-Cypate exhibited a relatively prolonged retention of NIRF signals in the tumor during the imaging period of 5 days (Figure 6D), accompanying with low NIRF noise from some major normal tissues such as lung, kidney and spleen after 24 h post-injection (Figure 6C).[9,19] The accumulation of GO-Cypate in tumor and its rapid clearance from normal tissues are highly advantageous to photothermal therapy with lower adverse side effect.[1d] Additionally, although GO-Cypate exhibited FRET effect upon irradiation, it also indicates that there were still some residual NIRF signals from GO-Cypate at tumor, which are also advantageous to achieve imaging-guided photothermal treatment.

2.3.2. Anticancer Efficacy

To elucidate the in vivo synergistic efficacy of GO-Cypate via pH-responsive photothermal effect under PTT treatment, GO-Cypate and GO-PEG were injected into the mice bearing 4T1 tumor at the single dose of 7.5 mg kg^{-1} Cypate, and then the tumors were treated with 785 nm photoirradiation at 24 h post-injection.[9] Subsequently, the tumor volumes were monitored for up to 22 days. The tumor volumes were normalized against their original volumes (0 day) to monitor the tumor growth (**Figure 7**A). The control group (PBS) with or without photoirradiation exhibited 30.0-fold increase of average tumor volumes compared to their original volumes, indicating that photoirradiation itself has a negligible influence on tumor growth. On the other hand, GO-Cypate and GO-PEG without photoirradiation also displayed a similar tumor growth behavior to that of the control group, and could be considered as nontoxic agents in the darkness.[9] However, GO-Cypate and GO-PEG exhibited a significant photothermal injury on the tumors under 785 nm PTT treatment, and triggered the tumor necrosis after 2 days post-injection. It indicates that sufficient amounts of GO-PEG and GO-Cypate were delivered into the tumors and thus induced obvious hyperthermia. But we subsequently found that GO-PEG exhibited obvious tumor re-growth during 8–22 days post-injection, and finally resulted in a 5.4-fold increase of tumor

© 2014 WILEY-VCH Verlag GmbH & Co. KGaA, Weinheim

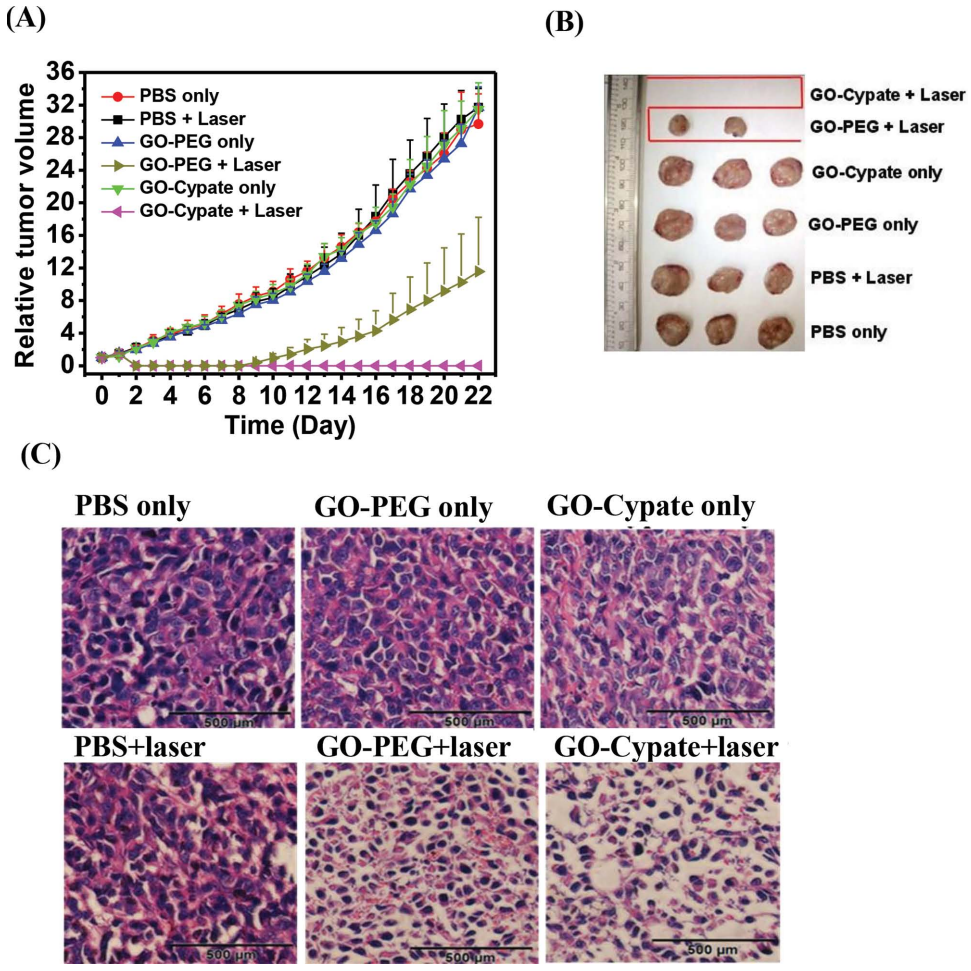

Figure 7. A) Tumor growth inhibition profiles of the mice bearing 4T1 tumor injected with GO-Cypate and GO-PEG at the dose of 7.5 mg kg^{-1} Cypate, respectively, followed by 785 nm PTT treatments (5 min, 1.0 W cm^{-2}) at 24 h post-injection ($n = 3$). B) Photos of the tumors extracted from the mice bearing 4T1 tumor at the end of the experiment (GO-Cypate exhibited complete tumor ablation and GO-PEG exhibited obvious tumor re-growth, $n = 3$). C) Images of H&E-stained tumor sections harvested from different groups of mice at 6 h post-photoirradiation.

volume (Figure 7B), indicating that GO-PEG could not completely eradicate the tumors. Most importantly, GO-Cypate caused the necrosis and regression of tumors at 2 days post-injection upon photoirradiation, and simultaneously achieved complete tumor ablation without any re-growth during 22 days post-injection (Figure 7B), which accords with the enhanced in vitro cytotoxicity as shown in Figure 5. Obviously, GO-Cypate exhibits a significant hyperthermia and tumor ablation owing to the sufficient tumor accumulation of GO-Cypate via EPR effect and enhanced photothermal cytotoxicity via FRET-enhanced photothermal effect. In addition, PTT does not require subcellular translocation of GO-Cypate, so the enhanced tumor accumulation and cellular uptake of GO-Cypate with enhanced photothermal performance can directly lead to superior tumor ablation.[9]

2.3.3. Ex Vivo Histological Staining

To further elucidate the in vivo synergistic damage of GO-Cypate against tumors under PTT treatment, various formulations including PBS, GO-PEG, and GO-Cypate were injected into the mice bearing 4T1 tumor at the single dose of 7.5 mg kg^{-1} Cypate, and then the tumors were treated with or without photoirradiation at 24 h post-injection, followed by hematoxylin-eosin (H&E) staining of tumor sections at 6 h post-photoirradiation. Figure 7C shows that GO-Cypate resulted in severe cancer necrosis and extensive hemorrhagicin flammation under PTT treatment, while GO-PEG only exhibited hemorrhagic inflammation and sporadic necrotic region surrounded by malignant cells with nuclear atypia. In contrast, PBS as the control did not exhibit obvious tumor necrosis with or without PTT treatment. On the other hand, GO-Cypate exhibited no significant toxicity on the normal tissues including heart, liver, spleen, lung and kidney without photoirradiation (Figure S8, Supporting Information). The results suggest that cyanine-grafted GO exhibits much more severe damage on tumor than GO-PEG alone.

3. Conclusion

In summary, we have successfully developed a pH-responsive GO-Cypate nanoplatform with enhanced photothermal effect

© 2014 WILEY-VCH Verlag GmbH & Co. KGaA, Weinheim

in lysosomal environment. Cypate molecules formed the aggregates on the surface of GO in aqueous solution, which generated additional photothermal energy from NIRF via pH-dependent FRET effect in addition to their original photothermal performances, and thus caused stronger photothermal cytotoxicity via FRET-enhanced hyperthermia. GO-Cypate displayed a good targeting capacity to tumor and finally resulted in more severe photothermal efficacy with tumor ablation. Obviously, photothermal agent with broad NIR absorbance as effective receptor of FRET can smartly improve the conversion of emitted NIRF energy from donor to the additional photothermal effect for improving PTT efficacy. These results suggest that cyanine-grafted GO is a promising pH-responsive photothermal nanoplatform via a FRET effect, which provides a new smart strategy to improve photothermal performance for superior PTT.

4. Experimental Section

Detailed experimental materials and methods can be found in the Supporting Information.

Supporting Information

Supporting Information is available from the Wiley Online Library or from the author.

Acknowledgements

M.G. and J.H. contributed equally to this work. This work was supported by National Basic Research Program (2014CB965003 and 2012CB932500), National Natural Science Foundation of China (31422021, 51473109, 21073224 and 51361130033), the priority academic program development of Jiangsu higher education institutions (PAPD), and Jiangsu Key Laboratory of Translational Research and Therapy for Neuro-Psycho-Diseases.

Received: August 13, 2014
Revised: September 11, 2014
Published online: October 13, 2014

[1] a) K. Yang, L. Feng, X. Shi, Z. Liu, *Chem. Soc. Rev.* **2013**, *42*, 530; b) Z. Zha, X. Yue, Q. Ren, Z. Dai, *Adv. Mater.* **2013**, *25*, 777; c) S. Lal, S. E. Clare, N. J. Halas, *Acc. Chem. Res.* **2008**, *41*, 1842; d) S. Luo, E. Zhang, Y. Su, T. Cheng, C. Shi, *Biomaterials* **2011**, *32*, 7127.

[2] a) E. C. Dreaden, A. M. Alkilany, X. Huang, C. J. Murphy, M. A. El-Sayed, *Chem. Soc. Rev.* **2012**, *41*, 2740; b) E. C. Dreaden, M. A. Mackey, X. H. Huang, B. Kang, M. A. El-Sayed, *Chem. Soc. Rev.* **2011**, *40*, 3391.

[3] a) D. K. Lim, A. Barhoumi, R. G. Wylie, G. Reznor, R. S. Langer, D. S. Kohane, *Nano Lett.* **2013**, *13*, 4075; b) A. F. Zedan, S. Moussa, J. Terner, G. Atkinson, M. S. El-Shall, *ACS Nano* **2013**, *7*, 627.

[4] a) M. Guo, H. Mao, Y. Li, A. Zhu, H. He, H. Yang, Y. Wang, X. Tian, C. Ge, Q. Peng, X. Wang, X. Yang, X. Chen, G. Liu, H. Chen, *Biomaterials* **2014**, *35*, 4656; b) Z. Wan, H. Mao, M. Guo, Y. Li, A. Zhu, H. Yang, H. He, J. Shen, L. Zhou, Z. Jiang, C. Ge, X. Chen, X. Yang, G. Liu, H. Chen, *Theranostics* **2014**, *4*, 399.

[5] a) P. Huang, C. Xu, J. Lin, C. Wang, X. Wang, C. Zhang, X. Zhou, S. Guo, D. Cui, *Theranostics* **2011**, *1*, 240; b) B. Tian, C. Wang, S. Zhang, L. Feng, Z. Liu, *ACS Nano* **2011**, *5*, 7000.

[6] a) H. Hong, K. Yang, Y. Zhang, J. W. Engle, L. Feng, Y. Yang, T. R. Nayak, S. Goel, J. Bean, C. P. Theuer, T. E. Barnhart, Z. Liu, W. Cai, *ACS Nano* **2012**, *6*, 2361; b) H. Hong, Y. Zhang, J. W. Engle, T. R. Nayak, C. P. Theuer, R. J. Nickles, T. E. Barnhart, W. Cai, *Biomaterials* **2012**, *33*, 4147; c) X. X. Ma, H. Q. Tao, K. Yang, L. Z. Feng, L. Cheng, X. Z. Shi, Y. G. Li, L. Guo, Z. Liu, *Nano Res.* **2012**, *5*, 199; d) K. Yang, L. L. Hu, X. X. Ma, S. Q. Ye, L. Cheng, X. Z. Shi, C. H. Li, Y. G. Li, Z. Liu, *Adv. Mater.* **2012**, *24*, 1868; e) Y. Sheng, X. S. Tang, E. W. Peng, J. M. Xue, *J. Mater. Chem. B* **2013**, *1*, 512; f) S. Kanakia, J. D. Toussaint, S. M. Chowdhury, G. Lalwani, T. Tembulkar, T. Button, K. R. Shroyer, W. Moore, B. Sitharaman, *Int. J. Nanomed.* **2013**, *8*, 2821; g) X. Shi, H. Gong, Y. Li, C. Wang, L. Cheng, Z. Liu, *Biomaterials* **2013**, *34*, 4786.

[7] a) D. Bitounis, H. Ali-Boucetta, B. H. Hong, D. H. Min, K. Kostarelos, *Adv. Mater.* **2013**, *25*, 2258; b) C. Chung, Y. K. Kim, D. Shin, S. R. Ryoo, B. H. Hong, D. H. Min, *Acc. Chem. Res.* **2013**, *46*, 2211; c) H. Shen, L. Zhang, M. Liu, Z. Zhang, *Theranostics* **2012**, *2*, 283; d) Y. Zhang, T. R. Nayak, H. Hong, W. Cai, *Nanoscale* **2012**, *4*, 3833; e) L. Zhang, Z. Lu, Q. Zhao, J. Huang, H. Shen, Z. Zhang, *Small* **2011**, *7*, 460; f) L. M. Zhang, J. G. Xia, Q. H. Zhao, L. W. Liu, Z. J. Zhang, *Small* **2010**, *6*, 537; g) K. Yang, S. A. Zhang, G. X. Zhang, X. M. Sun, S. T. Lee, Z. A. Liu, *Nano Lett.* **2010**, *10*, 3318; h) H. Wen, C. Dong, H. Dong, A. Shen, W. Xia, X. Cai, Y. Song, X. Li, Y. Li, D. Shi, *Small* **2012**, *8*, 760; i) L. Feng, X. Yang, X. Shi, X. Tan, R. Peng, J. Wang, Z. Liu, *Small* **2013**, *9*, 1989; j) K. Yang, Y. Li, X. Tan, R. Peng, Z. Liu, *Small* **2013**, *9*, 1492; k) K. Yang, J. Wan, S. Zhang, Y. Zhang, S. T. Lee, Z. Liu, *ACS Nano* **2011**, *5*, 516; l) Z. Sheng, L. Song, J. Zheng, D. Hu, M. He, M. Zheng, G. Gao, P. Gong, P. Zhang, Y. Ma, L. Cai, *Biomaterials* **2013**, *34*, 5236.

[8] a) Z. Liu, J. T. Robinson, X. Sun, H. Dai, *J. Am. Chem. Soc.* **2008**, *130*, 10876; b) X. Sun, Z. Liu, K. Welsher, J. T. Robinson, A. Goodwin, S. Zaric, H. Dai, *Nano Res.* **2008**, *1*, 203.

[9] H. Yang, H. Mao, Z. Wan, A. Zhu, M. Guo, Y. Li, X. Li, J. Wan, X. Yang, X. Shuai, H. Chen, *Biomaterials* **2013**, *34*, 9124.

[10] a) K. Miki, A. Kimura, K. Oride, Y. Kuramochi, H. Matsuoka, H. Harada, M. Hiraoka, K. Ohe, *Angew. Chem. Int. Ed.* **2011**, *50*, 6567; b) J. O. Escobedo, O. Rusin, S. Lim, R. M. Strongin, *Curr. Opin. Chem. Biol.* **2010**, *14*, 64; c) C. Zheng, M. Zheng, P. Gong, D. Jia, P. Zhang, B. Shi, Z. Sheng, Y. Ma, L. Cai, *Biomaterials* **2012**, *33*, 5603; d) M. Zheng, C. Yue, Y. Ma, P. Gong, P. Zhao, C. Zheng, Z. Sheng, P. Zhang, Z. Wang, L. Cai, *ACS Nano* **2013**, *7*, 2056.

[11] a) C. H. Lu, H. H. Yang, C. L. Zhu, X. Chen, G. N. Chen, *Angew. Chem. Int. Ed.* **2009**, *48*, 4785; b) Y. Wang, Z. Li, J. Wang, J. Li, Y. Lin, *Trends Biotechnol.* **2011**, *29*, 205.

[12] a) Y. Ye, W. P. Li, C. J. Anderson, J. Kao, G. V. Nikiforovich, S. Achilefu, *J. Am. Chem. Soc.* **2003**, *125*, 7766; b) Y. Ye, S. Bloch, J. Kao, S. Achilefu, *Bioconjug. Chem.* **2004**, *16*, 51.

[13] a) H. X. Chang, L. H. Tang, Y. Wang, J. H. Jiang, J. H. Li, *Anal. Chem.* **2010**, *82*, 2341; b) H. F. Dong, W. C. Gao, F. Yan, H. X. Ji, H. X. Ju, *Anal. Chem.* **2010**, *82*, 5511.

[14] a) H. Shen, M. Liu, H. X. He, L. M. Zhang, J. Huang, Y. Chong, J. W. Dai, Z. J. Zhang, *ACS Appl. Mater. Inter.* **2012**, *4*, 6317; b) Y. W. Wang, Y. Y. Fu, Q. L. Peng, S. S. Guo, G. Liu, J. Li, H. H. Yang, G. N. Chen, *J. Mater. Chem. B* **2013**, *1*, 5762.

[15] T. G. Iversen, T. Skotland, K. Sandvig, *Nano Today* **2011**, *6*, 176.

[16] F. Wang, Y. C. Wang, S. Dou, M. H. Xiong, T. M. Sun, J. Wang, *ACS Nano* **2011**, *5*, 3679.

[17] J. Huang, C. Zong, H. Shen, M. Liu, B. A. Chen, B. Ren, Z. J. Zhang, *Small* **2012**, *8*, 2577.

[18] H. Cabral, Y. Matsumoto, K. Mizuno, Q. Chen, M. Murakami, M. Kimura, Y. Terada, M. R. Kano, K. Miyazono, M. Uesaka, N. Nishiyama, K. Kataoka, *Nat. Nanotechnol.* **2011**, *6*, 815.

[19] J. Liu, M. Yu, C. Zhou, S. Yang, X. Ning, J. Zheng, *J. Am. Chem. Soc.* **2013**, *135*, 4978.

© 2014 WILEY-VCH Verlag GmbH & Co. KGaA, Weinheim